THE JOURNAL OF PHYSICAL CHEMISTRY A
A JOURNAL OF THE AMERICAN CHEMICAL SOCIETY

pubs.acs.org/JPCA Article

Acetone–Water Interactions in Crystalline and Amorphous Ice Environments

Published as part of The Journal of Physical Chemistry virtual special issue "10 Years of the ACS PHYS Astrochemistry Subdivision".

Michelle R. Brann, Stephen P. Hansknecht, Mark Muir, and S. J. Sibener*

Cite This: https://doi.org/10.1021/acs.jpca.2c01437 Read Online

ACCESS | Metrics & More | Article Recommendations

ABSTRACT: We present research that systematically examines acetone interacting with various D_2O ices of terrestrial and astrophysical interest using time-resolved, in situ reflection absorption infrared spectroscopy (RAIRS). We examine acetone deposited on top of different D_2O ice films: high-density, nonporous amorphous (np-ASW), and crystalline (CI) films as well as porous amorphous (p-ASW) with various pore morphologies. Analysis of RAIR spectra changes after acetone exposure, and we find that more hydrogen bonding occurs between acetone and p-ASW ices as compared to acetone and np-ASW or CI ices. Hydrogen bonding quantification occurred by two independent RAIR spectral changes: a greater relative intensity of the 1703 cm^{-1} feature at low acetone coverage as part of a 14 cm^{-1} shift in the C═O region and an ∼30% integrated dangling bond area reduction after acetone exposure. Interestingly, when changing the water structure to be more porous (deposited at 70° compared to 30°), there is a further reduction in the amount of hydrogen bonding that occurs. This suggests that there is a lack of access to surface sites with dangling bonds in the pores as initial layers of acetone block the pores and acetone is unable to diffuse within the structure at low temperatures. In general, these results offer a clearer picture of the mechanisms that can occur when small organic hydrocarbons interact with various icy interfaces; a quantitative understanding of these interactions is essential for the accurate modeling of many astrophysical processes occurring on the surface of icy dust particles.

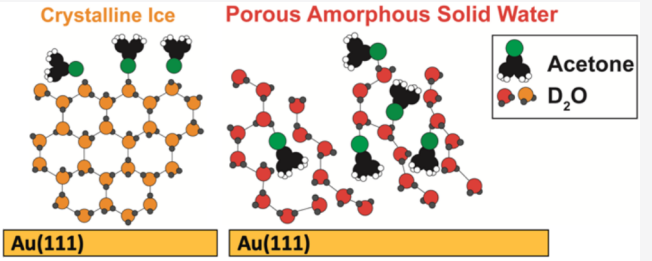

INTRODUCTION

Surface chemistry interactions between ices and small molecules are not as well understood as those that occur between adsorbates and metals.[1] These interactions are important for many atmospheric processes—such as reactions occurring on stratospheric cloud particles that can result in the seasonal ozone hole in Antarctica.[2,3] Additionally, bromine-induced tropospheric scavenging of ozone occurs on aerosols,[4−6] as well as midlatitude ozone depletion from volcanic eruptions.[7] Aside from atmospheric sciences, understanding chemical interactions and properties of astrophysical ices is important to help classify the composition and history of complex multicomponent ices.[8] Many interstellar dust grains are coated with thin ice films. Exposure to ultraviolet light, X-rays, cosmic radiation, or thermal processing can induce morphological changes resulting in novel molecules and increased chemical complexity.[9,10]

This work focuses on the interaction between acetone and astrophysical ices of varying morphologies: crystalline ice (CI), nonporous amorphous solid water (np-ASW), and porous amorphous solid water (p-ASW). CI ice in a hexagonal lattice is the most common form of snow and ice on Earth,[11] but it is also present in warmer astrophysical environments.[12] ASW, on the other hand, is the most abundant form of water in astrophysical environments[13] and is present in comets, planetary rings, and interstellar clouds.[14] ASW can be further classified into two types: high-density nonporous (np-ASW) and low-density porous (p-ASW) based on its pore structure.[15] In general, ASW morphology and accessibility to dangling bonds play a significant role in the adsorption and subsequent reactivity of volatile gas species within astrophysical ices.[16−19]

Acetone was chosen due to its relative abundance as a volatile organic in the troposphere,[1] its importance in organic chemistry, and its presence in the interstellar medium.[20] Acetone formation occurs on grain mantles where after gaseous CO molecules condense, they undergo hydrogen

Received: February 28, 2022
Revised: April 6, 2022

addition, resulting in formyl radicals.[21] These radicals can rapidly undergo addition reactions yielding methanol and acetaldehyde which upon reaction produce acetone. Thus, in order to quantify the role that acetone plays in icy dust grain mantles, it is necessary to classify how strongly acetone and water films interact.

More specifically, our work systematically probes acetone deposited on top of ice films of varying thicknesses as well as within a water matrix. This uniquely enables us to examine how the C═O moiety changes and therefore provides information about the film's orientation as well as hydrogen bonding effects. Our work builds upon experimental studies[22−26] as well as molecular dynamics simulations and *ab initio* calculations of the acetone−water system.[1,27] When investigating acetone adsorption on thin films (10−15 ML) of np-ASW and CI ices, Temperature-Programmed Desorption (TPD) measurements yielded two desorption states from the np-ASW film: a hydrogen bonded and a physiosorbed state. This is in contrast to only a physiosorbed state from the CI ice film. Therefore, acetone interacts with the np-ASW film more strongly than with CI ice due to the prevalence of hydrogen bonds. This is thought to be due to a structural difference between the np-ASW and CI ice films that impacts the ice's ability to form hydrogen bonds.[23]

Note that the surface chemistry of amorphous films is more complicated due to the presence of microscopic pores. Not only can species be trapped,[8] but also the deposition angle dictates the pore orientation and density.[28,29] Although there are many studies focused on adsorption into pores[14,16,29] to understand how pore morphology depends on the growth angle, little is known about how the pore morphology can impact hydrogen bonding sites and accessibility for adsorbed species to these sites.[30] Herein, we employ RAIRS to examine p-ASW and how its structure impacts diffusion and chemical interactions between acetone and the underlying film structure. We demonstrate that there are increased hydrogen bonding interactions between acetone and the p-ASW films, as compared to acetone and the np-ASW or CI films. Hydrogen bonding quantification occurred by observing two RAIR spectral changes: a greater relative intensity of the 1703 cm^{-1} feature at low acetone coverage as part of a 14 cm^{-1} shift in the C═O region and an ∼30% integrated dangling bond area reduction following exposure. Interestingly, when changing the water structure to be more porous (deposited at 70° compared to 30°), there is a further reduction in the amount of hydrogen bonding that occurs. Additionally, when examining dilute acetone inside a np-ASW matrix, we are able to tease apart peaks due to acetone interacting with water in the acetone−water interfacial region.

Overall, this work demonstrates that not only is there a difference in the ability to form hydrogen bonds between crystalline and amorphous water ices but also that such differences occur for porous amorphous water ices. Our work, therefore, demonstrates the importance of ice morphology in facilitating hydrogen bonding between interfacial under-coordinated water molecules and the C═O moiety. The demonstrated spectroscopic differences, particularly at sub-monolayer abundances, may guide the search for porous ices in the interstellar medium or on icy bodies in our solar system. Additionally, the prevalence of hydrogen bonds between acetone and crystalline and amorphous ices of varying porosity may impact subsequent reactivity and thus, molecular complexity and gas phase abundances of hydrocarbons. Aside from astrophysical environments, this work can also be applied more broadly to understand water and solid interfaces and the transport of these molecules into frozen media.

EXPERIMENTAL METHODS

All experiments were conducted in a molecular beam gas-surface scattering ultrahigh vacuum instrument that was previously discussed in detail.[31] This instrument consists of a UHV chamber with a base pressure of 10^{-10} Torr connected to a triply differentially pumped molecular beamline. In the main chamber, a He cooled manipulator (Advanced Research Systems) enables precise and accurate temperature control of the Au(111) sample between 16 and 800 K. The crystal is exposed to the beam and monitored in real time with optics for *in situ* reflection absorption infrared spectroscopy (RAIRS). Gas scattering and incident flux are monitored with a residual gas analyzer (RGA).

All RAIR spectra were analyzed using Gaussian peaks atop cubic baselines. Spectra were acquired with a Nicolet 6700 infrared spectrophotometer (Thermo Fisher) using incident *p*-polarized IR radiation at an angle of 75° to the Au(111) crystal and a liquid nitrogen cooled mercury cadmium telluride (MCT/A) detector. Each RAIR spectrum is an average of 200−300 scans taken using a 2 cm^{-1} resolution with a clean Au(111) sample or a D_2O underlayer for the background reference spectra.

D_2O films were produced via the directed doser at a 30° angle with respect to the surface normal and approximately 4 cm from the Au(111) crystal. The ice films used in this study varied between 100 and 600 layers thick. D_2O film thickness was determined by backfilling the UHV chamber to a chamber pressure of 1×10^{-7} Torr, which corresponds to a growth rate of 0.05 ML/s.[32] The D_2O growth and film thickness were monitored using RAIRS and integrated intensity of the O−D stretch between 3000 and 2000 cm^{-1}.[33] The deposition temperature of the Au(111) crystal determined the ice film coordination.[19,34] The D_2O films used in this study were np-ASW, p-ASW, or CI dosed at 108, 20, and 150 K, respectively. D_2O was typically leaked into the chamber at a pressure of 4×10^{-10} Torr, resulting in an average growth rate of ∼0.25 ML/s. ASW films with increased porosity were produced by increasing the angle of the directed doser relative to the surface normal from 30° to 70°.[35] The intensities of the dangling bond spectroscopic signals roughly scale with porosity so RAIR spectra can be used to qualitatively confirm that ices with different porosities have been formed.[36,37]

Figure 1 gives the normalized O−D stretch between 2200 and 2800 cm^{-1} for the three different ice films used in this study: np-ASW, p-ASW, and CI deposited at 108, 20, and 150 K, respectively, and collected at 68 K. When comparing acetone interacting with np-ASW, p-ASW, and CI D_2O films, it was necessary to anneal the films to a middle temperature of 68 K. This ensured that amorphous D_2O did not deposit on top of crystalline ice films during a lengthy cooling process to 20 K and that the porous film structure did not collapse and become nonporous at 108 K. As a result of D_2O molecule coordination differences among the films, we can easily distinguish p-ASW, np-ASW, and CI films.[38] Additionally, the p-ASW interface contains a significant fraction of three- and two-coordinated surface D_2O molecules ("dangling bonds") that are spectroscopically identified at 2725 and 2745 cm^{-1}, respectively.[39] Undercoordinated D_2O molecules not only change the density of the ASW structure but also can form hydrogen bonds with

https://doi.org/10.1021/acs.jpca.2c01437
J. Phys. Chem. A XXXX, XXX, XXX−XXX

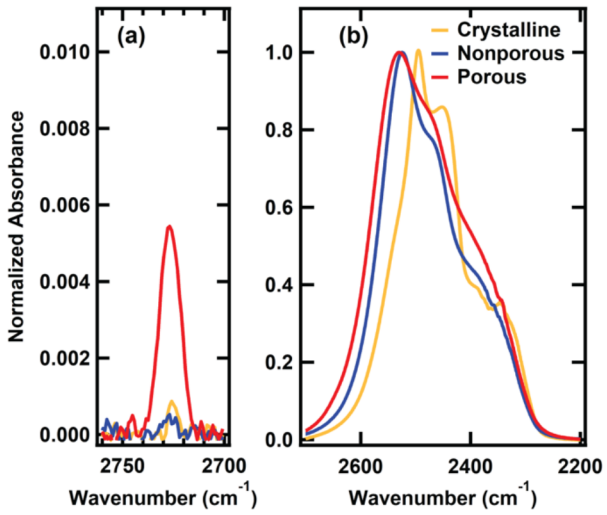

Figure 1. Normalized infrared spectra of 150 ML crystalline (CI, **yellow**), nonporous amorphous (np-ASW, **blue**), and porous amorphous (p-ASW, **red**) D_2O ices in the O−D stretch region between 2760 and 2700 cm^{-1} (a) and 2700 and 2200 (b) cm^{-1} dosed at 150, 108, and 20 K, respectively, and collected at 68 K. The region between 2760 and 2700 cm^{-1} (a) demonstrates that while dangling O−D are observed for all films, the intensity is greatest for the p-ASW films.

deposited acetone. On p-ASW films, there are two different surface sites that contain these dangling bonds: one on the top of the ice film and one decorating the pores. Annealing to 68 K for these experiments significantly reduced the number of two-coordinated surface molecules but does not change the number of three-coordinated molecules.

Although previous studies by Kimmel et al. demonstrated that N_2 TPD spectra obtained from films before and after annealing to ∼60 K differed in their line shape,[28] the total amount of N_2 adsorption was similar for both the deposited and annealed water film. This suggests that while annealing does result in some rearrangement of the molecules on the surface of the pores, this does not significantly adjust the overall porosity.[40] The np-ASW and CI ices also contain dangling bonds from surface molecules that are not fully participating in the hydrogen bonding network[41] but at a lower intensity compared to the p-ASW ice[29] (Figure 1a). On CI and np-ASW ices, there are only surface sites that contain dangling bonds available for hydrogen bonding on top of the ice film due to the lack of a pore structure. Due to the agreement in the integrated area of the 2730 cm^{-1} peak for the np-ASW and CI ices, the amount of dangling bonds of the surface of these two ices is similar but less than that of the surface of the p-ASW ice. Unless otherwise stated, p-ASW refers to the default porous film deposited at 30°, and other porous films (70°) will be labeled as such. When examining acetone interacting with p-ASW films of varying porosity, acetone exposure occurred at the deposition temperature (20 K).

Acetone (Sigma-Aldrich 99.5%, 5 °C) was bubbled through the molecular beam at a typical flux of 5.4×10^{14} molecules cm^{-2} s^{-1} that resulted in an average growth rate of 3 ML/min onto the Au(111) substrate or the D_2O ice film (assuming that one monolayer (ML) is $\sim 10^{15}$ molecules cm^{-2}).[32] The acetone molecular flux was determined by measuring the pressure rise using a nude Bayard-Albert ion gauge for an acetone beam open to the chamber. The flux was calculated by accounting for the relative gauge sensitivities to acetone and N_2,[42,43] the chamber pumping speed at different temperatures, and the beam spot size on the Au(111) crystal. By varying the pressure of the beam and monitoring the pressure rise for $m/z = 43$ amu measured by a RGA not in line with the beam and fitting to a linear regression, we determined the total acetone flux. The default acetone exposure was performed at normal incidence unless otherwise indicated.

For codosing experiments of D_2O and acetone, a 100-layer D_2O film was initially grown on the surface before D_2O was dosed through the directed doser, while the acetone was dosed through the supersonic molecular beam. Four different acetone film compositions were produced: 1%, 1.5%, 2%, and 25% where the acetone film percentage is calculated from the 1700 cm^{-1} C═O stretch for acetone and the 2200−2800 cm^{-1} OD stretch for D_2O. The acetone incident flux was reduced by employing a mechanical chopper (a rotating slotted disk). Concurrently, the directed doser's leak valve was adjusted to increase the D_2O growth rate. The final mixed D_2O and

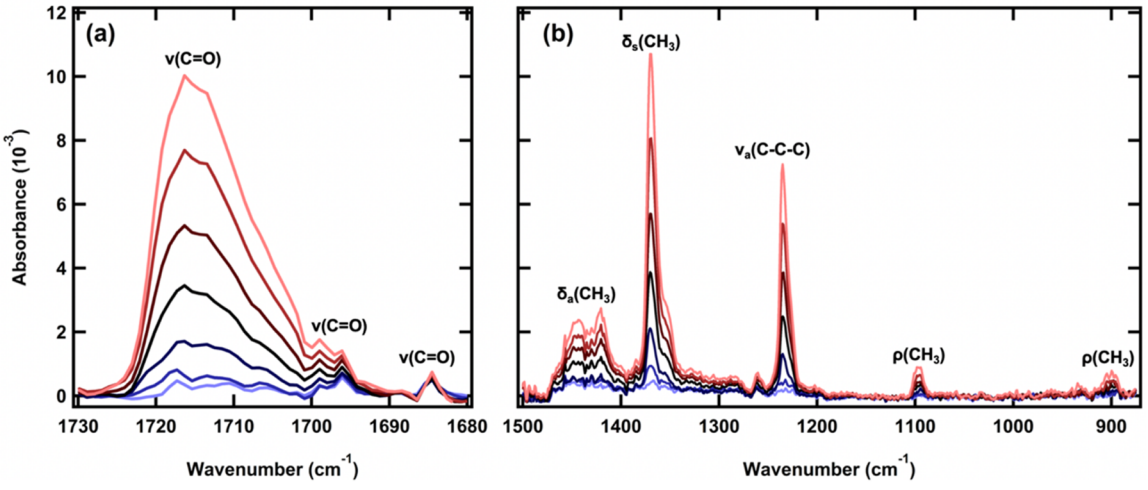

Figure 2. RAIR spectra of 1−24 ML of acetone adsorbed on Au(111) at 68 K. The RAIR spectra are separated into two wavenumber regimes: (a) C═O stretching between 1730 and 1680 cm^{-1} and (b) CH_3 deformation and rocking modes between 1500 and 875 cm^{-1}. The spectra correspond to 1, 1.7, 4.2, 8.3, 13, 19, and 24 ML of acetone.

https://doi.org/10.1021/acs.jpca.2c01437
J. Phys. Chem. A XXXX, XXX, XXX−XXX

acetone film were comprised of 400 layers of D_2O and between 4 and 50 layers of acetone. After dosing the mixed acetone and D_2O film, each RAIR spectrum is an average of 3000 scans.

RESULTS

Acetone Spectra. RAIR spectra of condensed amorphous acetone on Au(111) at 70 K is shown in Figure 2. In the condensed phase acetone spectra red-shifts as compared to liquid and gas phase spectra[44,45] and are comprised of many spectral features. The most intense spectral feature (in the 1700 region, Figure 2a) is assigned to the C═O stretch.[46−49] There are additional major spectral features corresponding to δ_a asymmetric methyl bending (1420 cm^{-1}), δ_s symmetric methyl bending (1371 cm^{-1}), v_a asymmetric C−C−C stretching (1239 cm^{-1}), and ρ methyl rocking (1097 cm^{-1}, 901 cm^{-1}) modes (Figure 2b).[46] Condensed phase acetone spectral features are red-shifted compared to the liquid features which are 1712 cm^{-1} (CO stretch), 1438 cm^{-1} (asymmetric methyl bending), 1420 cm^{-1} (asymmetric methyl bending), 1362 cm^{-1} (symmetric methyl bending), and 1092.5 cm^{-1} (methyl rocking). Unless otherwise stated, changes in the intensity and specific peak locations within the C═O region will be used to characterize acetone-substrate interactions.

As shown in Figure 2a, as layers of acetone grow in at 68 K, the C═O stretch splits into multiple peaks; and the peaks less than 1700 cm^{-1} saturate at low coverage, while the 1716 and 1708 components increase significantly with increasing acetone film thickness. These results show good agreement with previous RAIRS studies of acetone on Au(111) at 90 K[46] and FTIR studies of amorphous and crystalline acetone.[47] Therefore, this indicates that peaks at 1708 and 1716 cm^{-1} correspond to acetone−acetone bulk interactions,[23,26,50] whereas the 1694 and 1698 cm^{-1} peaks correspond to interfacial acetone.[49] It is important to note for our future analysis of acetone on top of and within water matrices that since the 1698−1708 cm^{-1} peaks are present in bulk condensed acetone, these features cannot be attributed to H-bonded CO as in liquid spectra of acetone and water mixtures.[44]

Low Coverage Acetone on Water Films of Varying Thickness. Next, we examined low coverage (<1 ML) of acetone dosed on top of np-ASW D_2O films of varying thickness (100, 300, 600 ML) at 108 K. All acetone films are between 0.74 and 0.94 ML of acetone. As shown in Figure 3, acetone on top of a 100 ML np-ASW D_2O film contains two features: a main acetone monolayer peak[23,46] at 1702 cm^{-1} and a shoulder at 1711 cm^{-1}. Since the 1711 cm^{-1} peak is attributed to multilayer acetone or acetone−acetone interactions,[51] this suggests that when the ASW film is thinner, fewer acetone molecules interact with water in the acetone−water interfacial region and that the water film is not yet self-similar; by self-similarity we mean that the structure of the interface is no longer varying with changes in thickness. Films less than 100 layers contain small islands that with increasing thickness converge to form a uniform film structure.[14,33,52−54] Thus, in contrast to the ultrathin films grown in previous studies,[22−24] we chose to grow ice films of at least 150 layers to ensure that any differences observed with how acetone interacts with the CI, np-ASW, and p-ASW D_2O ices are due to the underlying water coordination and not simply a film thickness effect.

Acetone Interaction with CI, np-ASW, and p-ASW Ice Films. To understand the interaction between acetone and our different astrophysical ices, we dosed layers of acetone on top of 150 layers of p-ASW, np-ASW, and CI films at 68 K and collected RAIR spectra. At 68 K, acetone and water desorption are unlikely to occur, and acetone is likely amorphous.[20,30,47] As seen in Figure 4a−c focused on the C═O region, each spectrum is normalized to the intensity at 1711.5 cm^{-1}, the amorphous multilayer carbonyl band,[47] to examine peak widths and shape as a function of exposure.

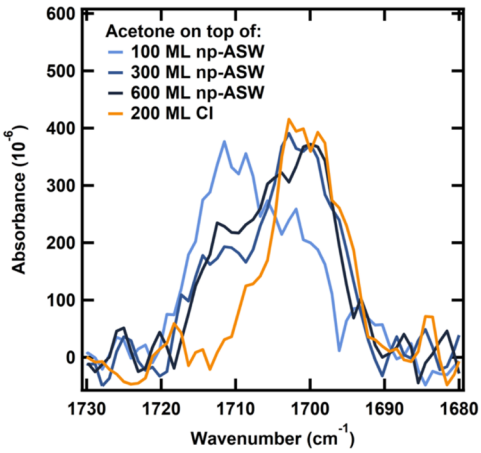

Figure 3. Representative RAIR spectra of the ν(CO) region of submonolayer acetone on top of np-ASW (**blue**) and CI (**orange**) D_2O films of varying thicknesses at 108 K. The thinnest np-ASW film (100 layers) has increased acetone spectral intensity at 1711 cm^{-1} indicating less interaction with the underlying water film.

For all three of the molecular ices, there is a blue-shift as a function of increasing exposure. This shift is consistent with acetone−acetone interactions in addition to the initial acetone−water substrate interactions. With increasing acetone exposure, the relative intensity of these low-frequency modes saturates as there is a larger growth of the bulk carbonyl modes (>1711 cm^{-1}). As an example, for acetone on p-ASW ices, the initial 2.6 ML spectra contain no spectra features greater than 1711.5 cm^{-1}. However, with increasing acetone exposure, new features grow in at 1712 and 1716 cm^{-1}. By 25 ML (spectra 6), the integrated area from the multilayer features (>1711.5 cm^{-1}) reaches ∼50% of that of the entire C═O region from 1680 to 17230 cm^{-1}. The relative ratio of ∼50% for the integrated area of features <1711.5 cm^{-1} and ∼50% for integrated area of features >1711.5 cm^{-1} remains relatively consistent throughout the rest of the exposure. In other words, with more than 25 ML of acetone, there is no change to the normalized acetone spectra for acetone on p-ASW, np-ASW, and CI ice films at 68 K with increasing exposure (Figure 4a−c). As shown in Figure 4c, for the p-ASW ices at low coverage, there is a 14 cm^{-1} shift to ∼1703 cm^{-1} when compared to the bulk value of 1717 cm^{-1}, indicative of hydrogen bonding between the ice to the carbonyl oxygen on the acetone.[25] This spectroscopic shift is also identified for acetone on top of np-ASW and CI ices. However, at low coverages of acetone, the relative intensity of the 1703 cm^{-1} mode is greatest for acetone on top of the p-ASW film followed by acetone on np-ASW and lastly acetone on CI.

We examine this further by focusing on the uncoordinated OD dangling bonds (Figure 4d−f) both after deposition and following acetone adsorption. After exposure to acetone, in the RAIR spectra between 2700 and 2800 cm^{-1}, there is a decrease in intensity of the OD dangling bond for all three ice films (CI,

https://doi.org/10.1021/acs.jpca.2c01437
J. Phys. Chem. A XXXX, XXX, XXX−XXX

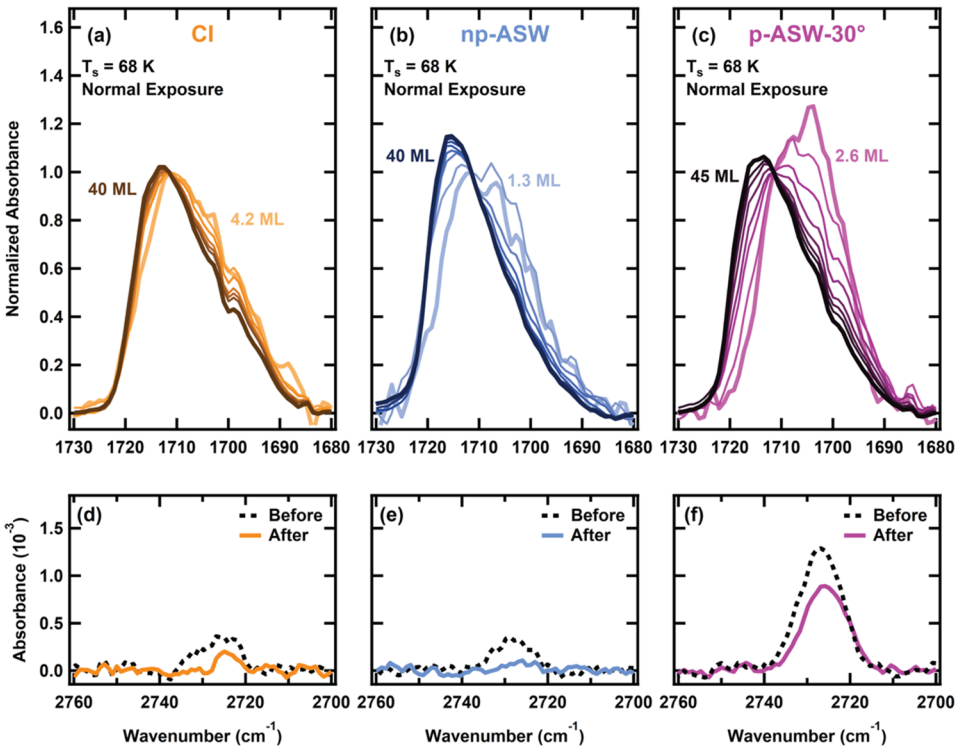

Figure 4. Representative RAIR spectra of the ν(CO) region of acetone on top of 150 layers of CI (a, **orange**), np-ASW (b, **blue**), and p-ASW (c, **pink**) D_2O films at 68 K. Acetone exposure was normal. All acetone spectra are normalized to the intensity at 1711.5 cm^{-1}, the amorphous multilayer carbonyl band. The initial and final acetone spectra for each D_2O film are slightly thicker, and with increasing acetone exposure, the spectra darken in color. Additional RAIR spectra (d–f) provide the corresponding OD dangling bond intensity before (----) and after (—) acetone exposure for the corresponding CI (d), np-ASW (e), and p-ASW (f) D_2O films. The 14 cm^{-1} shift (c) and decrease in dangling bond intensity (f) indicate increased hydrogen bonding occurs between uncoordinated D_2O molecules in the pores of p-ASW and the acetone.

np-ASW, and p-ASW), with the largest drop for the p-ASW films. Quenching of the dangling bond intensity occurs when the undercoordinated OD molecules hydrogen bond to the acetone. For CI and np-ASW films, this drop in dangling bond intensity results from acetone adsorbing onto available surface sites on top of the film. However, for p-ASW films, this drop in dangling bond intensity results from both acetone adsorbing onto available surface sites on top of the film as well as onto available sites that decorate the pore structure. In general, uncoordinated water molecules on the surface of the water film and within the open pore structure are necessary for hydrogen bonding to occur.[55,56] The larger drop in the higher wavenumber shoulder (2725 cm^{-1}) of the dangling bond peak for the p-ASW film after exposure suggests that acetone is more easily able to hydrogen bond to the less coordinated water molecules, possibly due to geometric presentation of the pores to the direction of the incident acetone beam.

Quantifying this further, we also focus on the integrated intensity of the OD dangling bonds between 2700 and 2800 cm^{-1} (Figure 5). For the np-ASW and CI films, the integrated OD dangling bond area after deposition is identical such that both films have the same number of dangling surface molecules.[26] After exposure to acetone at 68 K, this dangling bond feature diminishes slightly more for the acetone on top of np-ASW films as compared to acetone on top of CI films. Due to the fact that the CI dangling bond intensity does decrease after adsorption of acetone coupled with the presence of the 1703 cm^{-1} feature at low coverages of acetone, we conclude that hydrogen bonding does occur between the crystalline ice surface and acetone. However, since the relative intensity of

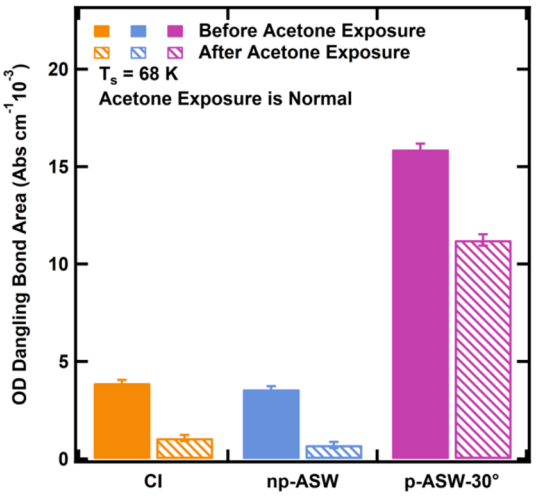

Figure 5. Integrated OD dangling bond intensity for CI (**orange**), np-ASW (**blue**), and p-ASW (**pink**) D_2O before and after exposure to 40–45 ML of acetone at 68 K. Due to its increased porosity, p-ASW films have more uncoordinated dangling bonds throughout the water film and thus form more hydrogen bonds with the underlying structure.

the 1703 cm^{-1} feature for acetone on CI ices is less than that for acetone on np-ASW ices, and more dangling bonds remain uncoordinated following exposure, fewer hydrogen bonds form between CI ices and acetone as compared to np-ASW ices and acetone.

https://doi.org/10.1021/acs.jpca.2c01437
J. Phys. Chem. A XXXX, XXX, XXX–XXX

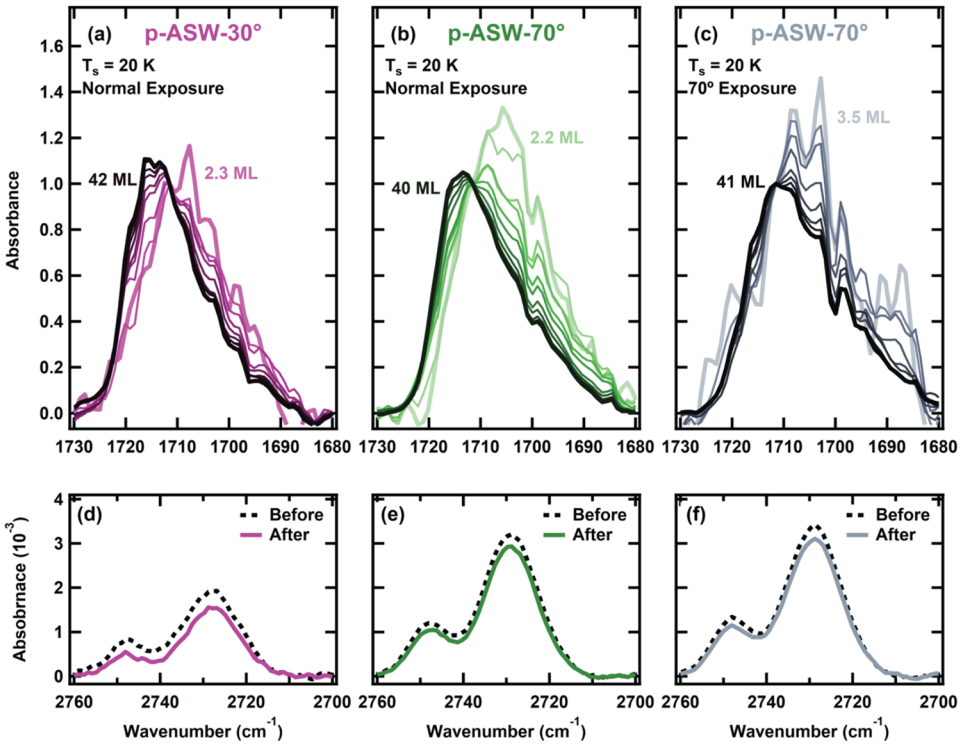

Figure 6. Representative RAIR spectra of the ν(CO) region of acetone on top of 150 layers of p-ASW D_2O films (a, **pink**) deposited at 30° and p-ASW D_2O films deposited at 70° (b, **green** c, **gray**) at 20 K. Acetone exposure was normal for **a** and **b** and 70° for **c**. All acetone spectra are normalized to the intensity at 1711.5 cm^{-1}, the amorphous multilayer carbonyl band. The initial and final acetone spectra for each D_2O film are slightly thicker, and with increasing acetone exposure, the spectra darken in color. Additional RAIR spectra (**d**–**f**) provide the corresponding OD dangling bond intensity before (----) and after (—) acetone exposure for the p-ASW D_2O films.

We suggest that the structural features of the CI surface are such that some of the uncoordinated OD molecules are not accessible for hydrogen bonding due to the rigid structure and the adsorption temperature. The np-ASW ice surface is rough on the length scale of several molecules, while the CI surface is much smoother. One possibility is that on CI ice films, the available surface sites with dangling bonds are oriented such that acetone is unable to form a linear bond with the planar ice surface and also experience significant van der Waals and electrostatic interactions with the film.[23] For low coverages of acetone at 68 K (Figure 4a–c), the spectroscopic feature at ~1709 cm^{-1} is assigned to van der Waals interactions[26] that occur between carbon atoms and all three difference D_2O films. Since additional electrostatic interactions occur between acetone and surface water molecules, not all free OD molecules may be able to form hydrogen bonds with acetone.

Regardless of the slight surface structural differences that occur between CI and np-ASW that dictate the amount of hydrogen bonds that can form, the p-ASW film has many more dangling bonds both on the surface and in the pores resulting in the largest integrated area compared among the three films (Figure 5). In other words, the p-ASW film has more available surface sites for hydrogen bonding. Upon exposure to acetone, the integrated area decreases by ~30% as acetone decorates the pore structure and adsorbs on top of the film. *Thus, we confirm due to the greatest relative intensity for the 1703 cm^{-1} feature* (Figure 4c) *and the largest titration of free OD molecules* (Figure 5) *that more hydrogen bonds occur between the p-ASW film and acetone as compared to acetone and the np-ASW or CI films.*

Acetone Interaction with p-ASW Films, Increased Porosity. To further probe the role that surface and pore sites with dangling bonds play in facilitating hydrogen bonds, we examined acetone dosed on top of 150 layers of p-ASW at 20 K (Figure 6a,d). We also examined acetone on top of p-ASW films with increased porosity (panels **b and c** for the acetone RAIR spectra and corresponding panels **e and f** for the OD dangling bonds).

First, we can see in the Figure 6d inset that as a result of not annealing the p-ASW D_2O film to 68 K, there is a new spectroscopic feature at 2748 cm^{-1} attributed to two coordinated D_2O molecules.[36] Additionally, the overall dangling bond surface area is greater than that of the p-ASW film annealed to 68 K. Similarly to the p-ASW film at 68 K (Figure 4d), upon exposure to acetone at 20 K, there is a decrease in dangling bond intensity as acetone is able to hydrogen bond to the ice surface. The hydrogen bonding is confirmed by the 14 cm^{-1} shift to 1703 cm^{-1} when compared to the bulk value of 1717 cm^{-1}. When further examining the intensity of the OD dangling bonds before and after exposure to acetone (Figure 6d), it is apparent that there is a greater decrease in the intensity of the higher wavenumber (2748 cm^{-1}), two coordinated D_2O molecules. This indicates that accessibility of free OD is necessary to facilitate the hydrogen bonding. The unannealed p-ASW film contains a larger integrated dangling bond intensity and, thus, has more sites available on the surface of the ice and within the pore structure that are available for hydrogen bonding. Interestingly, when comparing between the p-ASW at 20 K to the film annealed to 68 K, the same percentage (~30%) of dangling bonds participates in hydrogen bonding to acetone molecules (Figure

https://doi.org/10.1021/acs.jpca.2c01437
J. Phys. Chem. A XXXX, XXX, XXX–XXX

7). We suggest then, that acetone is unable to fully access the full canted pore structure[29] and is limited by the dangling

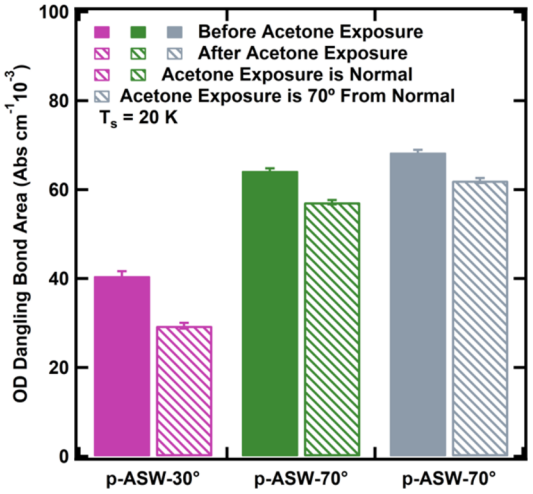

Figure 7. Integrated OD dangling bond intensity for p-ASW (**pink**) D_2O deposited at 30° and p-ASW (**green, gray**) deposited at 70° before and after exposure to 40−42 ML of acetone at 20 K. Acetone exposure occurred at normal incidence (**pink, green**) and at 70° (**gray**). Although there is a greater number of dangling OD molecules for films deposited at 70°, less overall hydrogen bonding occurs.

bonds that are accessible on the interfacial region. Since O−O distances in amorphous water samples deposited at 77 K can be ∼2.7 Å,[57] while acetone is closer to 3 Å, it is possible that acetone's size as well as the cryogenic experimental temperature (20 K) limits its mobility within the pore structure. To confirm this, we examined acetone on top of ASW films with increased porosity.

The ASW films with increased porosity were produced by changing the angle of the directed doser relative to the surface normal.[14,28,35] As we demonstrated previously[19] and characterized by Stevenson et al.,[14] porosity increases with the deposition angle such that D_2O films dosed at 30° are less porous than those grown at 60° or 70°.[58] These pores grow in at an orientation dictated by the deposition angle.[28] Additionally, since the intensities of the dangling bond spectroscopic signals scale with porosity, RAIR spectra can be used to qualitatively confirm that ices with different porosities have been formed.[36,37] p-ASW-70° films still contain the two different surface sites with dangling bonds available for hydrogen bonding: one on top of the ice film and one decorating the pores. However, since the p-ASW-70° film structure has larger pores, there are fewer surface sites on top of the ice film and more surface sites decorating the pores. To highlight the effect that pore structure has on hydrogen bonding, we choose to focus on acetone deposited on top of p-ASW films dosed at 70° since these films have the largest percentage of available undercoordinated surface sites that could hydrogen bond to the acetone.

We first compare the C═O RAIR stretch for acetone on top of p-ASW deposited at 70° to that deposited at 30° (Figure 6a,b). There are two noticeable spectral differences: the presence of the shoulder at 1720 cm^{-1} for high acetone coverages on the p-ASW-30° film and the higher relative broad intensity of the 1705 cm^{-1} feature for low coverages on the p-ASW-70° film. Both differences are attributed to the increased surface area of the 70° film.

Adjusting the dosing angle for the p-ASW from 30° to 70° also significantly increases the integrated area of the dangling bonds (Figure 7). Upon exposure of the p-ASW dosed at 70° to acetone at 20 K, the integrated OD dangling area decrease (and thus the amount of hydrogen bonding that occurs) is less than half that for the p-ASW dosed at 30° (Figure 5). This finding is supported by our previous work examining the methane sticking probability on p-ASW of varying morphologies (30°, 60°, 70°, and background deposited).[19] When examining total coverage scaled by the dangling bond surface area to give an approximate "fractional coverage", we determined that although the initial sticking probability was consistent across the different porous films, the relative methane accumulation was 1−2 times higher for background deposited and 30° films compared to those deposited at 60° or 70°. Although films deposited at 30° have less total surface area (from the integrated dangling bond intensity), their pores are closer to perpendicular to the substrate.[14,59] We suggest then that the difference in the number of hydrogen bonds that form results from the accessibility of different surface sites for hydrogen bonding. Since the p-ASW-70° films contain less surface sites on the top of the ice film and also form fewer hydrogen bonds as compared to the p-ASW-30° film, this indicates that these sites are readily available to the beam and extremely important for hydrogen bonding.

To test whether accessible surface sites to the beam are responsible for this difference, we deposited p-ASW films at 70° prior to acetone exposure also at 70° from the surface normal. As shown in Figure 7, the integrated dangling bond intensity decrease following exposure at 70° is comparable to the decrease that occurs from after exposure to an acetone beam normal to the surface. Thus, the same number of hydrogen bonds form between acetone and the p-ASW-70° film regardless of the angle of the incident acetone beam. In sum, this behavior results from a lack of access to available sites within the pores but *not* because of surface sites available to the beam. Since there was no difference in the number of hydrogen bonds that occur as a function of the incident beam deposition angle, it is likely that acetone covering the ice surface prevents additional acetone molecules from being able to access the entire pore structure. Since N_2 only readily diffuses into the pore structure at 23 K,[60] and NH_3 and CH_3OH are unable to diffuse into the pore structure,[61] it is not expected that acetone would diffuse at 20 K. Regardless of the beam's incident angle, once an acetone molecule adsorbs onto the surface, the surface temperature does not provide enough mobility to the molecule.

We conclude that increasing the surface dangling bonds for p-ASW films compared to CI and np-ASW films increases the number of hydrogen bonds occurring between acetone and the underlying p-ASW surface. When increasing the porosity of film (deposited at 70° compared to 30°), there is a further reduction in the number of hydrogen bonds, but this effect is not dependent on the angle of the incident acetone beam. Therefore, this results from a lack of access to available surface sites decorating the pores. Initial layers of acetone block the pores, and acetone is unable to diffuse through the structure at low temperatures. Overall, our results highlight the important role that interfacial uncoordinated OD dangling bonds play in facilitating hydrogen bonding especially between porous amorphous ices and acetone.

Acetone in a Nonporous Water Matrix, Concentration Effects. In order to examine individual acetone RAIR

https://doi.org/10.1021/acs.jpca.2c01437
J. Phys. Chem. A XXXX, XXX, XXX−XXX

spectra features, we also focused on acetone condensed in a np-ASW matrix. For these experiments, we first dosed ∼100 layers of np-ASW on the Au(111) before codosing acetone and np-ASW through both the beam and directed doser, respectively, at 108 K. By varying the incident acetone and water fluxes, this produces mixed films that ranged from 1 to 25% acetone. As shown in Figure 8, there are distinct RAIR spectral differences due to acetone concentration. There is a greater intensity of the 1698 cm^{-1} peak in the 1−2% acetone mixed films compared to the 25% acetone film due to isolation of individual acetone molecules. The relative intensity of this peak (1698 cm^{-1}) also decreases with increasing acetone percentage. There is also a red-shift of the 1711.5 cm^{-1} mode in the 25% acetone film when compared to the 1−2% films. Since the OH stretch band of liquid water surrounded by acetone was less red-shifted compared to pure liquid water,[44] this suggests that the acetone−water hydrogen bonding is weaker than the water−water hydrogen bonding in the mixed matrix.

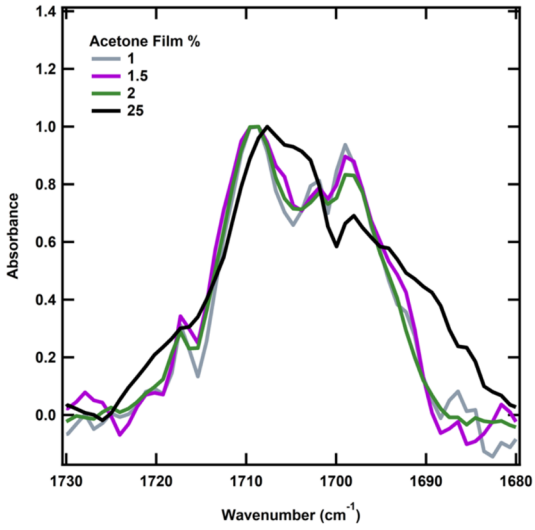

Figure 8. RAIR spectra of the ν(CO) region of acetone diluted in a np-ASW matrix at 108 K. The percentage of acetone in each mixture ranges from 1% (**gray**) to 25% (**black**). All acetone spectra are normalized to the intensity at 1708 cm^{-1}.

CONCLUSION

In this work, we present RAIR spectra analyses for acetone on top of D_2O ice films of varying morphologies and for acetone within an ice matrix. When first examining acetone on Au(111), we determine that the acetone spectra are comprised of both bulk (1708 cm^{-1}, 1716 cm^{-1}) and interfacial (1694 cm^{-1}, 1698 cm^{-1}) signatures that can be used to probe the strength and interaction between acetone and D_2O ice films. For low coverages (<1 ML) of acetone deposited on top of np-ASW and CI films, we determine that when the np-ASW film is thinner, less of the acetone molecules are interacting with water in the acetone−water interfacial region and that films are not structurally self-similar until 150 layers. Importantly, when increasing the underlying D_2O surface thickness and examining acetone on top of p-ASW, np-ASW, and CI films at 68 K, we conclude that more hydrogen bonding occurs between acetone and p-ASW ices as compared to acetone and np-ASW or CI films. Hydrogen bonding quantification occurred by two independent RAIR spectral changes: a greater relative intensity of the 1703 cm^{-1} feature at low acetone coverage as part of a 14 cm^{-1} shift in the C═O region and by an ∼30% integrated dangling bond area reduction following exposure. Interestingly, when changing the water structure to be more porous (deposited at 70° compared to 30°), there is a further reduction in the amount of hydrogen bonding that occurs. However, when adjusting the acetone deposition angle to match that of the angled pore structure, the number of hydrogen bonds formed is the same as that from a normal incidence beam striking the same surface (p-ASW-70°). Therefore, acetone is unable to access available surface sites in the pores due to initial adsorption blocking the pore structure at temperatures where acetone cannot diffuse.

In general, these results are further evidence that the morphology of the ice critically impacts the strength of the surface−adsorbate interactions and, thus, subsequent reactivity of incident molecules. Even if not fully porous, small cracks and morphological deformities in the surface of the astrophysical ices can lead to uncoordinated water molecules that hydrogen bond to incident projectiles. Strong hydrogen bonding between adsorbates and p-ASW ices may result in a higher desorption temperature of these molecules[62] thereby impacting comet outgassing, chemical abundances due to reactions in the ISM, and thermal and electrical processing of icy dust grains.[29]

AUTHOR INFORMATION

Corresponding Author

S. J. Sibener − *The James Franck Institute and Department of Chemistry, The University of Chicago, Chicago, Illinois 60637, United States;* orcid.org/0000-0002-5298-5484; Email: s-sibener@uchicago.edu

Authors

Michelle R. Brann − *The James Franck Institute and Department of Chemistry, The University of Chicago, Chicago, Illinois 60637, United States;* orcid.org/0000-0002-9889-3921

Stephen P. Hansknecht − *The James Franck Institute and Department of Chemistry, The University of Chicago, Chicago, Illinois 60637, United States*

Mark Muir − *The James Franck Institute and Department of Chemistry, The University of Chicago, Chicago, Illinois 60637, United States*

Complete contact information is available at: https://pubs.acs.org/10.1021/acs.jpca.2c01437

Notes

The authors declare no competing financial interest.

ACKNOWLEDGMENTS

This work was supported by the Air Force Office of Scientific Research, Grant FA9550-19-1-0324. This work was also supported in part by the Advanced Materials for Energy-Water Systems (AMEWS) Center, an Energy Frontier Research Center funded by the US Department of Energy, Office of Science, Basic Energy Sciences. S.P.H. acknowledges support from an NSF Alliances for Graduate Education and Professoriate supplement to grant CHE-1900188. Infrastructure support from the NSF-Materials Research Science and Engineering Center at the University of Chicago, Grant No. NSF-DMR-2011854, is also gratefully acknowledged.

https://doi.org/10.1021/acs.jpca.2c01437
J. Phys. Chem. A XXXX, XXX, XXX−XXX

REFERENCES

(1) Picaud, S.; Hoang, P. N. M. Adsorption of Acetone Molecules on Proton Ordered Ice. A Molecular Dynamics Study. *J. Chem. Phys.* **2000**, *112*, 9898−9908.

(2) Solomon, S. The Mystery of the Antarctic Ozone "Hole". *Rev. Geophys.* **1988**, *26*, 131−148.

(3) Orlando, J. J.; Tyndall, G. S. Laboratory Studies of Organic Peroxy Radical Chemistry: An Overview with Emphasis on Recent Issues of Atmospheric Significance. *Chem. Soc. Rev.* **2012**, *41*, 6294−6317.

(4) Fan, S.-M.; Jacob, D. J. Surface Ozone Depletion in Arctic Spring Sustained by Bromine Reactions on Aerosols. *Nat.* **1992**, *359*, 522−524.

(5) Finlayson-Pitts, B. J.; Livingston, F. E.; Berko, H. N. Ozone Destruction and Bromine Photochemistry at Ground Level in the Arctic Spring. *Nat.* **1990**, *343*, 622−625.

(6) Pershin, A. A.; Torbin, A. P.; Mikheyev, P. A.; Kaiser, R. I.; Mebel, A. M.; Azyazov, V. N. Ozone Destruction Due to the Recombination of Oxygen Atoms. *J. Chem. Phys.* **2021**, *155*, 164307.

(7) Brasseur, G.; Granier, C. Mount Pinatubo Aerosols, Chlorofluorocarbons, and Ozone Depletion. *Science* **1992**, *257*, 1239−1242.

(8) Ayotte, P.; Smith, R. S.; Stevenson, K. P.; Dohnálek, Z.; Kimmel, G. A.; Kay, B. D. Effect of Porosity on the Adsorption, Desorption, Trapping, and Release of Volatile Gases by Amorphous Solid Water. *J. Geophys. Res. Planets* **2001**, *106*, 33387−33392.

(9) Burke, D. J.; Brown, W. A. Ice in Space: Surface Science Investigations of the Thermal Desorption of Model Interstellar Ices on Dust Grain Analogue Surfaces. *Phys. Chem. Chem. Phys.* **2010**, *12*, 5947−5969.

(10) Palumbo, M. E.; Baratta, G. A.; Rangel, C.; Da Cruz, N. C.; Fulvio, D.; Garozzo, M.; Gomis, O.; Leto, G.; Spinella, F.; Strazzulla, G. Ion Irradiation of Astrophysical Ices. *J. Phys. Conf. Ser.* **2008**, *101*, 012002.

(11) Al-Halabi, A.; van Dishoeck, E. F.; Kroes, G. J. Sticking of CO to Crystalline and Amorphous Ice Surfaces. *J. Chem. Phys.* **2004**, *120*, 3358−3367.

(12) Jenniskens, P.; Blake, D. F. Crystallization of Amorphous Water Ice in the Solar System. *Astrophys. J.* **1996**, *473*, 1104−1113.

(13) Jenniskens, P.; Blake, D. F.; Kouchi, A. Amorphous Water Ice. In *Solar System Ices*; Springer: Dordrecht, 1998; pp 139−155, DOI: 10.1007/978-94-011-5252-5_7.

(14) Stevenson, K. P.; Kimmel, G. A.; Dohnalek, Z.; Smith, R. S.; Kay, B. D. Controlling the Morphology of Amorphous Solid Water. *Science* **1999**, *283*, 1505−1507.

(15) Angell, C. A. Amorphous Water. *Annu. Rev. Phys. Chem.* **2004**, *55*, 559−583.

(16) Smith, R. S.; Petrik, N. G.; Kimmel, G. A.; Kay, B. D. Thermal and Nonthermal Physiochemical Processes in Nanoscale Films of Amorphous Solid Water. *Acc. Chem. Res.* **2012**, *45*, 33−42.

(17) Bossa, J.-B.; Isokoski, K.; Paardekooper, D. M.; Bonnin, M.; van der Linden, E. P.; Triemstra, T.; Cazaux, S.; Tielens, A. G. G. M.; Linnartz, H. Porosity Measurements of Interstellar Ice Mixtures Using Optical Laser Interference and Extended Effective Medium Approximations. *Astron. Astrophys.* **2014**, *561*, A136.

(18) Isokoski, K.; Bossa, J.-B.; Triemstra, T.; Linnartz, H. Porosity and Thermal Collapse Measurements of H_2O, CH_3OH, CO_2, and H_2O:CO_2 Ices. *Phys. Chem. Chem. Phys.* **2014**, *16*, 3456−3465.

(19) Thompson, R. S.; Brann, M. R.; Sibener, S. J. Sticking Probability of High-Energy Methane on Crystalline, Amorphous, and Porous Amorphous Ice Films. *J. Phys. Chem. C* **2019**, *123*, 17855−17863.

(20) Almeida, G. C.; Pilling, S.; Andrade, D. P. P.; Castro, N. L. S.; Mendoza, E.; Boechat-Roberty, H. M.; Rocco, M. L. M. Photodesorption and Photostability of Acetone Ices: Relevance to Solid Phase Astrochemistry. *J. Phys. Chem. C* **2014**, *118*, 6193−6200.

(21) Millar, T. J.; Herbst, E.; Charnley, S. B. The Formation of Oxygen-Containing Organic Molecules in the Orion Compact Ridge. *Astrophys. J.* **1991**, *369*, 147.

(22) Schaff, J. E.; Roberts, J. T. The Adsorption of Acetone on Thin Films of Amorphous and Crystalline Ice. *Langmuir* **1998**, *14*, 1478−1486.

(23) Schaff, J. E.; Roberts, J. T. Toward an Understanding of the Surface Chemical Properties of Ice: Differences between the Amorphous and Crystalline Surfaces. *J. Phys. Chem.* **1996**, *100*, 14151−14160.

(24) Schaff, J. E.; Roberts, J. T. Structure Sensitivity in the Surface Chemistry of Ice: Acetone Adsorption on Amorphous and Crystalline Ice Films. *J. Phys. Chem.* **1994**, *98*, 6900−6902.

(25) Zhang, X. K.; Lewars, E. G.; March, R. E.; Parnis, J. M. Vibrational Spectrum of the Acetone-Water Complex: A Matrix Isolation FTIR and Theoretical Study. *J. Phys. Chem.* **1993**, *97*, 4320−4325.

(26) Mitlin, S.; Leung, K. T. Surface Chemistry of OH Dangling Bonds in Vapour-Deposited Ice Films at 128−185 K: Hydrogen-Bonding Interactions with Acetone. *Surf. Sci.* **2002**, *505*, L227−L236.

(27) Marinelli, F.; Allouche, A. An Ab Initio Study of Acetone and Formaldehyde Monolayers Adsorbed on Ice. *Chem. Phys.* **2001**, *272*, 137−147.

(28) Kimmel, G. A.; Stevenson, K. P.; Dohnalek, Z.; Smith, R. S.; Kay, B. D. Control of Amorphous Solid Water Morphology Using Molecular Beams. I. Experimental Results. *J. Chem. Phys.* **2001**, *114*, 5284−5294.

(29) Kimmel, G. A.; Dohnálek, Z.; Stevenson, K. P.; Smith, R. S.; Kay, B. D. Control of Amorphous Solid Water Morphology Using Molecular Beams. II. Ballistic Deposition Simulations. *J. Chem. Phys.* **2001**, *114*, 5295−5303.

(30) Souda, R. Adsorption, Diffusion, Dewetting, and Entrapment of Acetone on Ni(111), Surface-Modified Silicon, and Amorphous Solid Water Studied by Time-of-Flight Secondary Ion Mass Spectrometry and Temperature Programmed Desorption. *J. Chem. Phys.* **2011**, *135*, 164703.

(31) Gibson, K. D.; Killelea, D. R.; Yuan, H.; Becker, J. S.; Sibener, S. J. Determination of the Sticking Coefficient and Scattering Dynamics of Water on Ice Using Molecular Beam Techniques. *J. Chem. Phys.* **2011**, *134*, 034703.

(32) Callen, B. W.; Griffiths, K.; Memmert, U.; Harrington, D. A.; Bushby, S. J.; Norton, P. R. The Adsorption of Water on Ni(110): Monolayer, Bilayer and Related Phenomena. *Surf. Sci.* **1990**, *230*, 159−174.

(33) Killelea, D. R.; Gibson, K. D.; Yuan, H.; Becker, J. S.; Sibener, S. J. Dynamics of the Sputtering of Water from Ice Films by Collisions with Energetic Xenon Atoms. *J. Chem. Phys.* **2012**, *136*, 144705.

(34) Smith, R. S.; Petrik, N. G.; Kimmel, G. A.; Kay, B. D. Thermal and Nonthermal Physiochemical Processes in Nanoscale Films of Amorphous Solid Water. *Acc. Chem. Res.* **2012**, *45*, 33−42.

(35) Dohnálek, Z.; Kimmel, G. A.; Ayotte, P.; Smith, R. S.; Kay, B. D. The Deposition Angle-Dependent Density of Amorphous Solid Water Films. *J. Chem. Phys.* **2003**, *118*, 364−372.

(36) Buch, V.; Devlin, J. P. Spectra of Dangling OH Bonds in Amorphous Ice: Assignment to 2- and 3-Coordinated Surface Molecules. *J. Chem. Phys.* **1991**, *94*, 4091−4092.

(37) Cholette, F.; Zubkov, T.; Smith, R. S.; Dohnálek, Z.; Kay, B. D.; Ayotte, P. Infrared Spectroscopy and Optical Constants of Porous Amorphous Solid Water. *J. Phys. Chem. B* **2009**, *113*, 4131−4140.

(38) Bergren, M. S.; Schuh, D.; Sceats, M. G.; Rice, S. A. The OH Stretching Region Infrared Spectra of Low Density Amorphous Solid Water and Polycrystalline Ice Ih. *J. Chem. Phys.* **1978**, *69*, 3477−3482.

(39) Accolla, M.; Congiu, E.; Dulieu, F.; Manicò, G.; Chaabouni, H.; Matar, E.; Mokrane, H.; Lemaire, J. L.; Pirronello, V. Changes in the Morphology of Interstellar Ice Analogues after Hydrogen Atom Exposure. *Phys. Chem. Chem. Phys.* **2011**, *13*, 8037−8045.

(40) Horimoto, N.; Kato, H. S.; Kawai, M. Stepwise Morphological Change of Porous Amorphous Ice Films Observed through Adsorption of Methane. *J. Chem. Phys.* **2002**, *116*, 4375−4378.

(41) Rowland, B.; Devlin, J. P. Spectra of Dangling OH Groups at Ice Cluster Surfaces and within Pores of Amorphous Ice. *J. Chem. Phys.* **1991**, *94*, 812−813.

https://doi.org/10.1021/acs.jpca.2c01437
J. Phys. Chem. A XXXX, XXX, XXX−XXX

(42) Itikawa, Y. Cross Sections for Electron Collisions with Nitrogen Molecules. *J. Phys. Chem. Ref. Data* **2006**, *35*, 31−53.
(43) Pastega, D. F.; Lange, E.; Ameixa, J.; Barbosa, A. S.; Blanco, F.; Garcia, G.; Bettega, M. H. F.; Limão-Vieira, P.; Ferreira de Silva, F. Combined Experimental and Theoretical Study on the Differential Elastic Scattering Cross Sections for Acetone by Electron Impact Energy of 7.0−50 EV. *Phys. Rev. A* **2016**, *93*, 032708.
(44) Max, J. J.; Chapados, C. Infrared Spectroscopy of Acetone-Water Liquid Mixtures. I. Factor Analysis. *J. Chem. Phys.* **2003**, *119*, 5632−5643.
(45) Rogers, J. D.; Rub, B.; Goldman, S.; Person, W. B. Measurement of Infrared Intensities for Fundamental Vibrations of Gaseous Acetone. *J. Phys. Chem.* **1981**, *85*, 3727−3729.
(46) Syomin, D.; Koel, B. E. IRAS Studies of the Orientation of Acetone Molecules in Monolayer and Multilayer Films on Au(111) Surfaces. *Surf. Sci.* **2002**, *498*, 53−60.
(47) Hudson, R. L.; Gerakines, P. A.; Ferrante, R. F. IR Spectra and Properties of Solid Acetone, an Interstellar and Cometary Molecule. *Spectrochim. Acta Part A Mol. Biomol. Spectrosc.* **2018**, *193*, 33−39.
(48) Andrade, D. P. P.; De Barros, A. L. F.; Ding, J.; Rothard, H.; Boduch, P.; da Silveira, E. F. Acetone Degradation by Cosmic Rays in the Solar Neighbourhood and in the Galactic Centre. *Mon. Not. R. Astron. Soc.* **2014**, *444*, 3792−3801.
(49) Shin, S.; Kang, H.; Kim, J. S.; Kang, H. Phase Transitions of Amorphous Solid Acetone in Confined Geometry Investigated by Reflection Absorption Infrared Spectroscopy. *J. Phys. Chem. B* **2014**, *118*, 13349−13356.
(50) Shin, S.; Kim, Y.; Kang, H.; Kang, H. Effect of Electric Field on Condensed-Phase Molecular Systems. I. Dipolar Polarization of Amorphous Solid Acetone. *J. Phys. Chem. C* **2015**, *119*, 15588−15595.
(51) Vannice, M. A.; Erley, W.; Ibach, H. A RAIRS and HREELS Study of Acetone on Pt(111). *Surf. Sci.* **1991**, *254*, 1−11.
(52) Kay, B. D.; Lykke, K. R.; Creighton, J. R.; Ward, S. J. The Influence of Adsorbate-Absorbate Hydrogen Bonding in Molecular Chemisorption: NH_3, HF, and H_2O on Au(111). *J. Chem. Phys.* **1989**, *91*, 5120−5121.
(53) Gibson, K. D.; Killelea, D. R.; Becker, J. S.; Yuan, H.; Sibener, S. J. Energetic Ballistic Deposition of Volatile Gases into Ice. *Chem. Phys. Lett.* **2012**, *531*, 18−21.
(54) Brann, M. R.; Thompson, R. S.; Sibener, S. J. Reaction Kinetics and Influence of Film Morphology on the Oxidation of Propene Thin Films by $O(^3P)$ Atomic Oxygen. *J. Phys. Chem. C* **2020**, *124*, 7205−7215.
(55) Nagasawa, T.; Sato, R.; Hasegawa, T.; Numadate, N.; Shioya, N.; Shimoaka, T.; Hasegawa, T.; Hama, T. Absolute Absorption Cross Section and Orientation of Dangling OH Bonds in Water Ice. *Astrophys. J. Lett.* **2021**, *923*, L3.
(56) Bahr, S.; Toubin, C.; Kempter, V. Interaction of Methanol with Amorphous Solid Water. *J. Chem. Phys.* **2008**, *128*, 134712.
(57) Narten, A. H.; Venkatesh, C. G.; Rice, S. A. Diffraction Pattern and Structure of Amorphous Solid Water at 10 and 77 K. *J. Chem. Phys.* **1976**, *64*, 1106.
(58) Smith, R. S.; Zubkov, T.; Dohnálek, Z.; Kay, B. D. The Effect of the Incident Collision Energy on the Porosity of Vapor-Deposited Amorphous Solid Water Films. *J. Phys. Chem. B* **2009**, *113*, 4000−4007.
(59) Hornekaer, L.; Baurichter, A.; Petrunin, V. V.; Field, D.; Luntz, A. C. Importance of Surface Morphology in Interstellar H_2 Formation. *Science* **2003**, *302*, 1943−1946.
(60) Rowland, B.; Devlin, J. P. Spectra of Dangling OH Groups at Ice Cluster Surfaces and within Pores of Amorphous Ice. *J. Chem. Phys.* **1991**, *94*, 812.
(61) Collings, M. P.; Anderson, M. A.; Chen, R.; Dever, J. W.; Viti, S.; Williams, D. A.; McCoustra, M. R. S. A Laboratory Survey of the Thermal Desorption of Astrophysically Relevant Molecules. *Mon. Not. R. Astron. Soc.* **2004**, *354*, 1133−1140.
(62) Bolina, A. S.; Brown, W. A. Studies of Physisorbed Ammonia Overlayers Adsorbed on Graphite. *Surf. Sci.* **2005**, *598*, 45−56.

https://doi.org/10.1021/acs.jpca.2c01437
J. Phys. Chem. A XXXX, XXX, XXX−XXX